

Quasi-angular momentum of Bose and Fermi gases in rotating optical lattices

Brandon M. Peden, Rajiv Bhat, Meret Krämer, and
Murray J. Holland

JILA, NIST and Department of Physics, University of Colorado, Boulder CO
80309-0440, USA

E-mail: pedenb@colorado.edu

Abstract. The notion of quasi-angular momentum is introduced to label the eigenstates of a Hamiltonian with a discrete rotational symmetry. This concept is recast in an operatorial form where the creation and annihilation operators of a Hubbard Hamiltonian carry units of quasi-angular momentum. Using this formalism, the ground states of ultracold gases of non-interacting fermions in rotating optical lattices are studied as a function of rotation, and transitions between states of different quasi-angular momentum are identified. In addition, previous results for strongly-interacting bosons are re-examined and compared to the results for non-interacting fermions. Quasi-angular momentum can be used to distinguish between these two cases. Finally, an experimentally accessible signature of quasi-angular momentum is identified in the momentum distributions of single-particle eigenstates.

1. Introduction

Recent experimental and theoretical studies of quantum gases of ultracold atoms have been successful in replicating the behavior of a wide class of condensed matter systems. In particular, Bose-Einstein condensation (BEC) [1, 2, 3] and the degenerate Fermi gas [4] have both been observed, and there have been extensive studies of superfluidity, vortex formation [5], and the BCS-BEC crossover [6, 7]. The Mott-insulator to superfluid phase transition in the Bose-Hubbard model has been observed in a system of ultracold bosons in an optical lattice of [8, 9].

Along these lines, focus has turned to strongly-correlated effects in ultracold atomic gases. In particular, a mapping between the Hamiltonian of electrons confined in two dimensions in the presence of a constant transverse magnetic field and that of a rotating atomic gas has led to various theoretical studies predicting fractional quantum Hall effect (FQHE) behavior in rotating BEC's [10, 11, 12, 13]. However, experimentally reaching the parameter regimes necessary to observe this behavior is difficult [14]. Optical lattices offer a solution to this problem by enhancing correlations. Optical lattices are formed as standing waves of counter-propagating laser beams and act as a lattice for ultracold atoms. These systems are highly tunable: lattice spacing and depth can be varied by tuning the frequency and intensity of the lasers, and interactions between atoms can be tuned via a Feshbach resonance. Some recent studies have made direct connections between FQHE physics and strongly-interacting bosons in optical lattices in the presence of an effective magnetic field [15, 16, 17, 18, 19].

Connecting these theoretical studies to experiment requires identifying observables that can act as experimental signatures for the predicted physics. For instance, linear response theory has been applied to current flow in the presence of a “potential gradient” in order to observe FQHE physics [18], noise correlation analysis has been applied to bosons in a rotating ring lattice [20], and Bragg spectroscopy has been mentioned as a probe for vortex states [21]. A common observable in ultracold atomic gases is the momentum distribution, measured in time-of-flight experiments.

In this paper, we present analytical results for strongly-interacting bosons in rotating optical lattices that confirm numerical results in a previous paper [22] and extend them to systems of non-interacting fermions. These results are based on the notion of quasi-angular momentum, which is a quantum number for systems with a discrete rotational symmetry. Quasi-angular momentum is analogous to quasi-momentum for periodic translationally invariant systems and has been previously used in the context of carbon nanotubes to label Bloch states [23]. A formalism for this quantum number for second-quantized systems is presented and applied to gases of bosons and fermions in rotating optical lattices. The results presented here identify transitions between states of different symmetry for the ground state of a rotating system. A possible avenue for experimentally detecting these results via the momentum distribution of the ground state is also presented.

The quasi-angular momentum, m , of the ground state of an ultracold quantum gas of strongly-interacting bosons or non-interacting fermions in a rotating ring lattice of N sites can be monitored as a function of rotation speed. For the case of strongly-interacting bosons, m cycles through the values $m = nl \bmod N : l = 0, 1, 2, \dots$, where n is the number of particles. For the case of fermions, m cycles through the values $m = nl \bmod N : l = 0, 1, 2, \dots$ for odd numbers of particles and $m = n(l + 1/2) \bmod N : l = 0, 1, 2, \dots$ for even numbers of particles. A system of non-

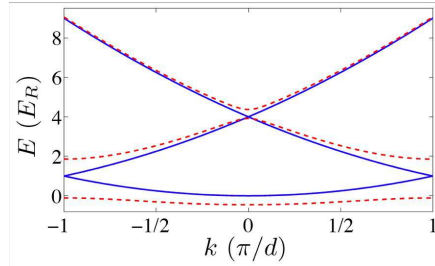


Figure 1. Dispersion relation for free particles (solid) and particles moving in a one-dimensional sinusoidal lattice (dashed) plotted in a reduced zone scheme. Free space dispersion relations are plotted versus momentum, and lattice dispersion relations are plotted versus quasi-momentum. Energy is in units of the recoil energy, $E_R = \hbar^2 \pi^2 / 2md^2$, where d is the lattice spacing.

interacting fermions is thereby distinguishable from a system of hard-core bosons. Similar behavior obtains for systems of fermions in two-dimensional square lattices. Signatures of this quantum number in experiment are observable via the momentum distribution of the ground state. For single-particle systems in two-dimensional square lattice geometries, such signatures include the existence of a peak at $\mathbf{k} = 0$ only for the $m = 0$ state and peak-spacing differences between $m = 2$ and $m = 1, 3$ state.

The paper is structured as follows. In section 2, we draw the analogy between systems with a discrete translational symmetry and systems with a discrete rotational symmetry, thereby generating a Bloch theory for the latter and introducing the notion of quasi-angular momentum. Specific investigations of quantum gases of strongly-interacting bosons and non-interacting fermions in ring and square lattice geometries are carried out in section 3. In section 4, signatures of the quasi-angular momentum in the momentum distribution of a state are identified. Section 5 summarizes the main results of the paper.

2. Quasi-angular momentum

In this section, we briefly review band theory and introduce the language of Bloch functions and quasi-momentum (see for instance [24, 25]). By analogy, the *quasi-angular momentum* of an eigenstate of a system with a discrete rotational symmetry is defined.

2.1. Bloch theory

When a small periodic potential of lattice period d is introduced to a free-particle system, the two wavefunctions $\psi_1(x) = e^{i\pi x/d}$ and $\psi_2(x) = e^{-i\pi x/d}$ at the Brillouin zone boundaries ($q = \pm\pi/d$) mix with each other. The potential acts as a perturbation that breaks the degeneracy between these two states, creating new eigenfunctions,

$$\psi_{\pm}(x) = \frac{1}{\sqrt{2}} \left(e^{i\pi x/d} \pm e^{-i\pi x/d} \right). \quad (1)$$

This process opens up a band-gap at the Brillouin zone boundaries. In a reduced zone scheme, this energy spectrum becomes the familiar one-dimensional Bloch band diagram (see figure 1).

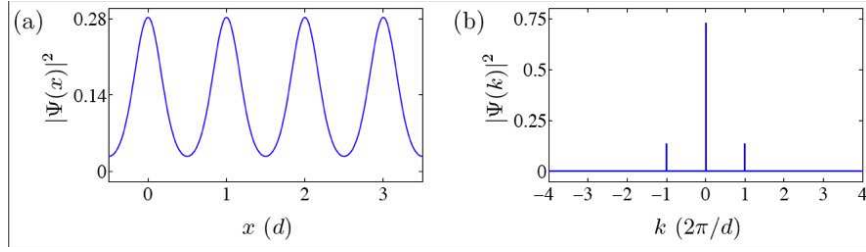


Figure 2. (Color online.) The zero quasi-momentum Bloch function in the first band for an infinite sinusoidal lattice if lattice depth $V_0 = 5E_R$. (a) The real space wave function is concentrated in the lattice sites. (b) The wave function in momentum space exhibits peaks at reciprocal lattice vectors. The envelope of these peaks is given by a Gaussian for large lattice depths, consistent with a lattice of simple harmonic oscillator wells.

The introduction of a periodic potential breaks the continuous translational symmetry of the system, and therefore the wavefunctions are no longer momentum eigenstates. Instead, the eigenfunctions of the Hamiltonian are eigenfunctions of a discrete translation operator, T_d , that translates the entire system by one lattice spacing,

$$\psi(x-d) = T_d \psi(x) = e^{-ikd} \psi(x), \quad (2)$$

and can be labeled by k , the *quasi-momentum*. A quasi-momentum eigenstate of a periodic Hamiltonian can be written as the product of a plane wave and a function periodic in the lattice:

$$\psi_k^{(l)}(x) = e^{ikx} u_k^{(l)}(x), \quad u_k^{(l)}(x-d) = u_k^{(l)}(x), \quad (3)$$

where l is a band index.

When these Bloch functions are expanded in the momentum basis, the only momenta contributing to the sum are those that differ from k by a reciprocal lattice vector, $G_j = \frac{2\pi j}{d}$. The expansion is then given by

$$\psi_k^{(l)}(x) = \int_{-\infty}^{\infty} \frac{dq}{\sqrt{2\pi}} e^{iqx} \psi_k^{(l)}(q) = \sum_{j=-\infty}^{\infty} c_j^{(l)} \frac{e^{i(k+2\pi j/d)x}}{\sqrt{2\pi}}, \quad (4)$$

where the expansion coefficients $c_j^{(l)}$ are given by

$$c_j^{(l)} = \int_{-\infty}^{\infty} dx \frac{e^{-i(k+2\pi j/d)x}}{\sqrt{2\pi}} \psi_k^{(l)}(x). \quad (5)$$

Figure 2(a) is an example of a Bloch function in a sinusoidal lattice, and figure 2(b) is the Fourier transform of this Bloch function – that is, the Bloch function in momentum space.

In the rest of the paper, we will consider only lattices that are deep enough that a single-band approximation will be adequate to describe the physics. In the proceeding sections, then, we drop the band index, l .

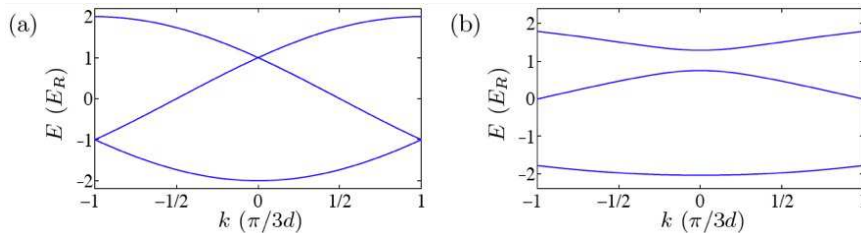


Figure 3. (Color online.) (a) Lowest band dispersion relation for a one-dimensional sinusoidal lattice plotted in a reduced zone scheme that anticipates the lowering of the symmetry via an additional potential with periodicity $3d$. (b) After the introduction of this potential, states with the same quasi-momentum, k in the reduced zone mix with each other, opening up gaps anywhere that there is a degeneracy.

2.2. Lowering the symmetry

If an extra potential, $V(x)$, satisfying

$$V(x - pd) = V(x), \quad (6)$$

with $p \geq 2$ an integer and d the lattice spacing, is introduced to a lattice, then Bloch states $\langle x|k\rangle = \psi_k(x)$ and $\langle x|k'\rangle = \psi_{k'}(x)$ will mix with each other if k and k' differ by $2\pi m/pd$, as shown by the following calculation:

$$\langle k'|V|k\rangle = \int_{-\infty}^{\infty} dx \psi_{k'}^*(x) V(x) \psi_k(x) = e^{i(k'-k)pd} \langle k'|V|k\rangle. \quad (7)$$

Eigenstates of the new Hamiltonian will therefore be linear combinations of these Bloch states. The potential increases the lattice periodicity and, accordingly, decreases the size of the first Brillouin zone to $2\pi/pd$.

In figure 3(a), the lowest band of a one-dimensional lattice with an arbitrary periodic potential is plotted in a reduced zone scheme. Introducing an infinitesimal potential whose periodicity is three times the lattice spacing d , the first Brillouin zone is reduced to the region $-\pi/3d \leq k \leq \pi/3d$. Equation (7) shows that the states lying on a vertical line in figure 3(b) mix with each other under the addition of the new potential – i.e., $\langle k'|V|k\rangle$ is non-zero for these states. In particular, the degenerate states at $k = 0$ mix, breaking the degeneracy and opening up a gap at $k = 0$, as shown in figure 3(b). The single band splits into three bands due to the reduction of the symmetry by $V(x)$.

When the addition of a potential reduces the symmetry of a system, as $V(x)$ did to the generic system described in figure 3, the original eigenstates of the system mix according to their symmetry. Accordingly, gaps open up where there are degeneracies between states of the same symmetry, creating a band structure.

2.3. The ground state of a moving lattice

The utility of these symmetry concepts and quasi-momentum can be demonstrated by considering the effect of moving the lattice. In a stationary lattice, a zero quasi-momentum Bloch function is always the ground state. When the lattice is moving, the energetically favored state is one that moves along with the lattice. In order to

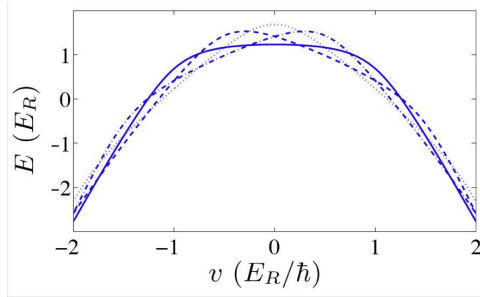


Figure 4. (Color online.) The four lowest energies in the single-particle energy spectrum as a function of lattice velocity for a four-site sinusoidal lattice with periodic boundary conditions. At zero velocity, the zero quasi-momentum state (solid) is the ground state. At some finite positive velocity, the $k = \pi/2d$ state (dashed) is energetically favorable and becomes the ground state. The ground state eventually cycles through all quasi-momenta.

investigate this phenomenon, we move to a frame co-moving with the lattice. The Hamiltonian in this frame is given by [26]

$$H = H_0 - \mathbf{p} \cdot \mathbf{v}, \quad (8)$$

where H_0 is the Hamiltonian in the non-moving frame, and \mathbf{v} is the velocity of the moving frame with respect to the lab frame. The ground state of $H_0 - \mathbf{p} \cdot \mathbf{v}$ will be the ground state of the lab frame but written in rotating frame coordinates.

Consider an eigenstate of H_0 , $\psi_k(x)$. In first-order perturbation theory, the energy of this state is

$$E_k = \langle k | H_0 - \mathbf{p} \cdot \mathbf{v} | k \rangle = E_k^0 - v \langle k | p | k \rangle. \quad (9)$$

At zero velocity, the ground state is a zero quasi-momentum state, $\psi_0(x)$. However, the energy of a state that has a positive average momentum, $\langle k | p | k \rangle > 0$, falls below that of $\psi_0(x)$ for large enough v . This change is signalled by an exact energy level crossing in the energy spectrum between two quasi-momentum states (see figure 4). As the velocity is increased, the effect of the velocity term is to reorder the energies of the quasi-momentum states, thereby leading to exact energy level crossings.

2.4. Quasi-angular momentum

A moving N -site linear lattice with periodic boundary conditions is analogous to a rotating N -site ring lattice. We can make this analogy explicit by considering the Hamiltonian of a moving, one-dimensional, sinusoidal N -site lattice in the co-moving frame, given by

$$H = -\frac{\hbar^2}{2M} \frac{\partial^2}{\partial x^2} + V_0 \cos^2(qx) - v \frac{\hbar}{i} \frac{\partial}{\partial x}, \quad (10)$$

where v is the velocity of the lattice. The wave-number q can be rewritten as $q = \pi/d$, where d is the lattice spacing. If periodic boundary conditions,

$$\psi(x + Nd) = \psi(x), \quad (11)$$

are included, then the Hamiltonian describes the system illustrated in figure 5(a) for the explicit case of an 8-site lattice. On the other hand, the Hamiltonian of a rotating, sinusoidal N -site ring lattice (figure 5(b)) in the rotating frame is given by

$$H = -\frac{\hbar^2}{2M} \frac{1}{R^2} \frac{\partial^2}{\partial \phi^2} + V_0 \cos^2 \left(N \frac{\phi}{2} \right) - \Omega \frac{\hbar}{i} \frac{\partial}{\partial \phi}, \quad (12)$$

where Ω is the rotation frequency, R is the radius of the ring, and $\frac{\hbar}{i} \frac{\partial}{\partial \phi}$ is the angular momentum operator, L_z . The inclusion of the term $-\Omega L_z$ has the effect of moving to a frame co-rotating with the lattice [26]. The two Hamiltonians, equations 10 and 12, are identical if we perform a transformation $x = \phi N d / 2\pi$ and identify $N d / 2\pi$ with R and v/R with Ω .

Since the Hamiltonians are exactly identical, all of the properties of one-dimensional systems with a discrete translational invariance carry over for ring systems with a discrete rotational invariance. The analogy can be carried further, starting with the two-dimensional free-space solution in polar coordinates,

$$\psi_j(\phi, \rho) = e^{ij\phi} R_j(\rho), \quad (13)$$

where $R_j(\rho)$ is a radial function, irrelevant for our discussion, and j is an integer. In the presence of a potential that breaks the rotational symmetry, the eigenstates are linear combinations of these free-space solutions. If this potential has a discrete N -fold rotational symmetry, its eigenstates can be expanded in the free space solutions as

$$\psi_m(\phi, \rho) = \sum_{j=-\infty}^{\infty} a_j e^{i(Nj+m)\phi} R_j(\rho). \quad (14)$$

It is evident from this expansion that $\psi_m(\phi, \rho)$ is an eigenvector with eigenvalue $e^{-i2\pi m/N}$ of the discrete rotation operator $R_{2\pi/N}$ that rotates the system by the angle $2\pi/N$; $R_{2\pi/N}$ takes the place of the discrete translation operator, T_d . The analogy is complete when we note that the eigenstates are linear combinations of angular momentum eigenstates, in which case we call the number $\hbar m$ the quasi-angular momentum of the state, $\psi_m(\phi, \rho)$. For the rest of the paper, we will drop the factor of \hbar from the quasi-angular momentum.

3. Bosons and fermions in rotating optical lattices

Interacting bosons in one dimension enter the Tonks-Girardeau regime when interactions get very strong [27, 28]. The gas takes on some of the characteristics of a gas of non-interacting fermions, such as an identical number density. It differs in certain aspects, however, such as the momentum distribution. It then becomes particularly interesting to compare the cases of strongly-interacting bosons and non-interacting fermions in rotating lattices. In this section, gases of non-interacting fermions and hard-core bosons in rotating optical lattices are investigated. A many-particle formalism is generated for quasi-angular momentum states and used to monitor the symmetry of the ground state as a function of rotation.

The Hamiltonian for interacting bosons or fermions in a rotating optical lattice takes the second quantized form,

$$H = \sum_{\sigma} \int d^D x \hat{\Psi}_{\sigma}^{\dagger}(\mathbf{x}) \left(-\frac{\hbar^2}{2M} \nabla^2 + V_0 \cos^2(\mathbf{k} \cdot \mathbf{x}) - \Omega L_z \right) \hat{\Psi}_{\sigma}(\mathbf{x}) \\ + \sum_{\lambda\lambda', \mu\mu'} \int d^D x \int d^D x' \hat{\Psi}_{\lambda}^{\dagger}(\mathbf{x}) \hat{\Psi}_{\lambda'}^{\dagger}(\mathbf{x}') V(\mathbf{x}, \mathbf{x}')_{\lambda\lambda', \mu\mu'} \hat{\Psi}_{\mu'}(\mathbf{x}) \hat{\Psi}_{\mu}(\mathbf{x}'), \quad (15)$$

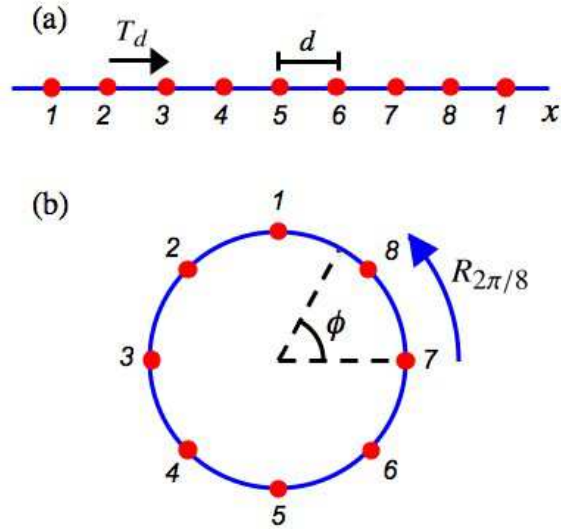


Figure 5. (Color online.) This diagram shows the equivalence between a one-dimensional lattice with periodic boundary conditions and a ring lattice with the same number of sites. The translation operator T_d that translates through one lattice site maps onto the rotation operator $R_{2\pi/8}$ that rotates the lattice through one lattice site.

where D is the dimension of the system, λ , μ , and σ are spin indices, and $\Psi_\sigma(\mathbf{x})$, $\Psi_\sigma^\dagger(\mathbf{x})$ are field operators satisfying the (anti-)commutation relations,

$$\begin{aligned} \left[\hat{\Psi}_\sigma(\mathbf{x}), \hat{\Psi}_{\sigma'}^\dagger(\mathbf{x}') \right]_{\pm} &= \delta_{\sigma\sigma'} \delta(\mathbf{x} - \mathbf{x}'), \\ \left[\hat{\Psi}_\sigma(\mathbf{x}), \hat{\Psi}_{\sigma'}(\mathbf{x}') \right]_{\pm} &= 0. \end{aligned} \quad (16)$$

Assuming spin-independent contact interactions, a Hubbard Hamiltonian can be derived in a lowest-band, tight-binding approximation by expanding the field operators in the lowest-band Wannier functions, $w(\mathbf{x} - \mathbf{x}_j)$ [29]. A basis better suited in the presence of rotation is given by the modified Wannier functions,

$$W_j(\mathbf{x}) = e^{-i\phi_{ij}} w(\mathbf{x} - \mathbf{x}_j), \quad \phi_{ij} = \frac{M}{\hbar} \int_{\mathbf{x}_j}^{\mathbf{x}_i} \mathbf{A}(\mathbf{x}') \cdot d\mathbf{x}' \quad (17)$$

where $\mathbf{A}(\mathbf{x}') = \boldsymbol{\Omega} \times \mathbf{x}'$ [30]. This modification captures the effect of rotation at low rotation speeds [30]; however, this approximation needs to be further modified at higher rotation speeds where the density of the Wannier functions is modified along with the phase. The phase, ϕ_{ij} , is a constant multiple of the rotation frequency for a ring lattice, in which case make the replacement, $-i\phi_{ij} \rightarrow i\Omega\Phi$.

The result for spinless bosons is [18]

$$\begin{aligned} H_B = & - \sum_{\langle i,j \rangle} \left(t + \frac{1}{2} M \Omega^2 A_1 \right) \left(e^{-i\phi_{ij}} a_i^\dagger a_j + e^{i\phi_{ij}} a_j^\dagger a_i \right) \\ & + \sum_j \left(\epsilon - \frac{1}{2} M \Omega^2 (r_j^2 + A_2) \right) a_j^\dagger a_j + \frac{U}{2} \sum_j a_j^\dagger a_j^\dagger a_j a_j. \end{aligned} \quad (18)$$

A similar derivation for spin-1/2 fermions yields

$$\begin{aligned}
 H_F = & - \sum_{\langle i,j \rangle, \sigma} \left(t + \frac{1}{2} M \Omega^2 A_1 \right) \left(e^{-i\phi_{ij}} a_{i,\sigma}^\dagger a_{j,\sigma} + e^{i\phi_{ij}} a_{j,\sigma}^\dagger a_{i,\sigma} \right) \\
 & + \sum_{j,\sigma} \left(\epsilon - \frac{1}{2} M \Omega^2 (r_j^2 + A_2) \right) a_{j,\sigma}^\dagger a_{j,\sigma} + \frac{U}{2} \sum_j a_{j,\uparrow}^\dagger a_{j,\downarrow}^\dagger a_{j,\downarrow} a_{j,\uparrow}. \quad (19)
 \end{aligned}$$

For both cases, i, j are site indices with $\langle i, j \rangle$ indicating a sum over only nearest neighbours; A_1, A_2, ϵ, U , and t are overlap integrals that can be numerically evaluated for a lattice of specific shape, period, and depth [18]; and r_i is the radial position of the i 'th site. If a harmonic trap is included, $\Omega^2 \rightarrow \Omega^2 - \Omega_T^2$, where Ω_T is the trap frequency.

In the rest of the paper, a lattice depth of $V_0 = 10E_R$ is assumed, and all parameters in the Hubbard Hamiltonians are numerically computed for this depth.

3.1. Strongly-interacting bosons

In this section, we describe hard-core bosons in a rotating optical lattice. The quasi-angular momentum of an eigenstate for a one-dimensional system is then defined and monitored as a function of rotation speed. The analytic results herein derived are consistent with a previous numerical treatment of a two-dimensional system [30].

In the limit of very strong interactions, $U \rightarrow \infty$, the two-state approximation becomes exact. In this *hard-core boson* regime, the occupation number of each site is between l or $l + 1$. We can encode this fact in the Hamiltonian by formally changing the properties of the creation and annihilation operators. Here we consider the case of filling factors less than one, as the results for higher filling factors are qualitatively identical (see the appendix for the general case). This can be effected by stipulating on-site anti-commutation relations for the operators – i.e.,

$$\left[a_i, a_i^\dagger \right]_+ = 1, \quad \left[a_i, a_{j \neq i} \right]_- = \left[a_i, a_{j \neq i}^\dagger \right]_- = 0. \quad (20)$$

In this case, the interaction term vanishes, although strong-interactions still implicitly exist in the Hamiltonian. For practical purposes, $U = 100t$, where t is the tunneling energy, is large enough to enter this regime [30].

The Hamiltonian for a ring-lattice is given by

$$\begin{aligned}
 H = & - \sum_{j=1}^N \left(t + \frac{M \Omega^2}{2} A_1 \right) e^{i\Omega\Phi} a_{j+1}^\dagger a_j + h.c. \\
 & + \sum_{j=1}^N \left(\epsilon - \frac{M \Omega^2}{2} M \Omega^2 (R^2 + A_2) \right) a_j^\dagger a_j, \quad (21)
 \end{aligned}$$

where R is the radius of the ring. This Hamiltonian can be diagonalized by first performing the Jordan-Wigner transformation [31, 32],

$$b_j = a_j e^{i\pi \sum_{i=1}^{j-1} a_i^\dagger a_i}, \quad (22)$$

which transforms the mixed a operators into fully fermionic ones. The transformed Hamiltonian takes different forms for even and odd numbers of particles. Performing the canonical transformation,

$$d_m = \frac{1}{\sqrt{N}} \sum_{j=1}^N e^{-i\pi f_m j / N} b_j, \quad (23)$$

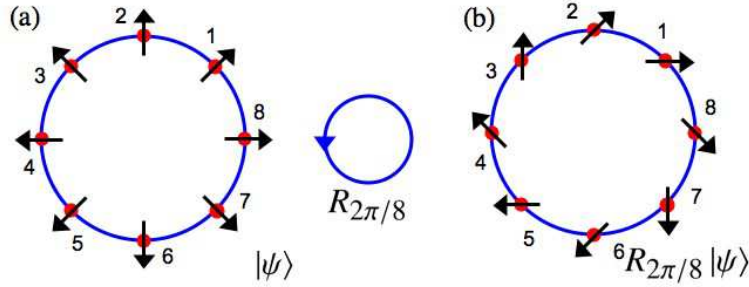


Figure 6. (Color online.) (a) The operator d_1^\dagger adds one particle to the system, populating every site with equal probability but a phase that differs by $2\pi/8$ between lattice sites. The state that is illustrated is $|\psi\rangle = d_1^\dagger |0\rangle$; arrows indicate phase. (b) When this state is rotated by one lattice site, the resulting state is $R_{2\pi/8} |\psi\rangle$. Subtracting the phases at a site before and after rotation, we get $\phi = -2\pi/8$. The picture then illustrates the fact that $|\psi\rangle$ is an eigenstate of $R_{2\pi/8}$ with eigenvalue $e^{-i2\pi/8}$.

where $f_m = 2m$ for n odd, $f_m = 2m - 1$ for n even, and n is the number of particles, results in

$$H = \sum_{m=1}^N E_m d_m^\dagger d_m, \quad (24)$$

$$E_m = -2 \left(t + \frac{1}{2} M \Omega^2 A_1 \right) \cos \left(\frac{\pi f_m}{N} - \Omega \Phi \right) + \epsilon - \frac{1}{2} M \Omega^2 (R^2 + A_2) \quad (25)$$

The eigenstates are of the form $d_{m_1}^\dagger \dots d_{m_n}^\dagger |0\rangle$.

A complete picture of this diagonalization requires an interpretation of the eigenstates in terms of quasi-angular momentum. The discrete rotation operator is defined via

$$R b_{j \neq N}^\dagger R^{-1} = b_{j+1}^\dagger, \quad R b_N^\dagger R^{-1} = (-1)^n b_1^\dagger, \quad R |0\rangle = |0\rangle. \quad (26)$$

This operator commutes with the Hamiltonian, and its action on an eigenstate, $|\psi\rangle = d_{m_1}^\dagger \dots d_{m_n}^\dagger |0\rangle$, is

$$R |\psi\rangle = e^{-i\pi(f_{m_1} + \dots + f_{m_n})/N} |\psi\rangle. \quad (27)$$

Therefore, the quasi-angular momentum of this state is $\left(\frac{f_{m_1} + \dots + f_{m_n}}{2} \right) \bmod N$. A pictorial representation of this discussion is shown in figure 6 for a specific case with one particle.

We are now in a position to use this formalism to investigate the ground state of the system. The ground state is determined by populating the lowest energy levels in the standard way for fermions. Equation 25 is the single-particle energy spectrum E_m . As Ω is increased, the minimum value of the cosine moves to the right, as illustrated in figure 7(a). The ground state is then determined by populating the lowest energy $d_m^\dagger d_m$ eigenstates. In figures 7(b) and 7(c), this process is illustrated for the case of three particles in an eight-site ring.

In general, if the minimum is near $m = m_0$, populate states $m_0, m_0 \pm 1, \dots, m_0 \pm p$ for $n = 2p + 1$ particles in the system. The quasi-angular momentum of the state is

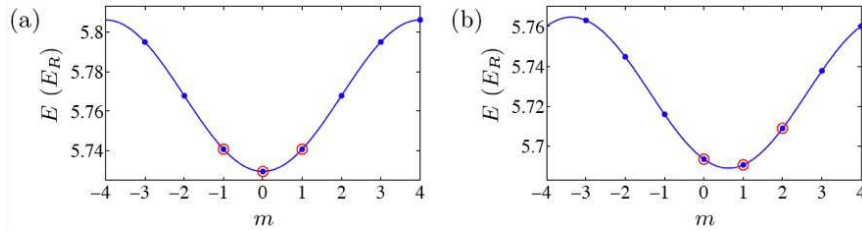


Figure 7. (Color online.) Ground state of three strongly-interacting bosons in a rotating 8-site ring lattice. Solid curves are guides for the eye. (a) At $\Omega = 0$, the three lowest single-particle energies carry quasi-angular momentum $m = -1, 0, 1$. The three-particle ground state therefore has quasi-angular momentum $m = (-1 + 0 + 1) \bmod 8 = 0$. (c) At $\Omega = 0.14 E_R / \hbar$, the three lowest single-particle energies carry quasi-angular momentum $m = 0, 1, 2$. The three-particle ground state therefore has quasi-angular momentum $m = (0 + 1 + 2) \bmod 8 = 3$.

then

$$m = \sum_{l=-p}^p (m_0 + l) \bmod N = m_0 (2p + 1) \bmod N = m_0 n \bmod N. \quad (28)$$

A similar argument holds for even numbers of particles. Thus, as rotation is increased from $\Omega = 0$, the quasi-angular momentum cycles through the values,

$$m = jn \bmod N : j = 0, 1, 2, \dots \quad (29)$$

One final note for the case of bosons. If there is an infinitesimal potential, V , that breaks the symmetry of the original Hamiltonian, H_0 , down to a four-fold rotational symmetry, the behavior described in section 2.2 obtains. We treat the problem perturbatively. Tiny bandgaps in the single-particle energy spectrum, equation 25, open up at the new Brillouin zone boundaries. The eigenstates of H_0 are independent of Ω . Therefore, to first order in V , the energy level shifts are independent of Ω , and the eigenstates remain unchanged. The effect of rotation is then exactly the same as in the non-perturbed case, and the quasi-angular momenta have the same behavior as a function of rotation. However, since the old quasi-angular momentum is no longer a good quantum number, we have to take

$$m \rightarrow m \bmod 4. \quad (30)$$

These results are consistent with the treatment in a previous paper [30].

3.2. Non-interacting fermions in a ring lattice

Previous results focused on strongly-interacting bosons in rotating optical lattices [22, 30]. Here, we describe non-interacting fermions in ring lattices and compare to the boson case. The quasi-angular momentum of the ground state changes as rotation is increased. The allowed values of this quantity for fermions differ from those of the boson case.

For non-interacting fermions, we drop the spin index, and the Hamiltonian for a ring lattice is identical to equation 21 except that the operators are fermionic. This Hamiltonian can be analytically diagonalized via the canonical transformation

$$d_m = \frac{1}{\sqrt{N}} \sum_{j=1}^N e^{-i2\pi m j / N} a_j. \quad (31)$$

The Hamiltonian is identical to that of equations 24 and 25 except that $f_m = 2m$ for both even and odd numbers of particles. The eigenstates, $d_{m_1}^\dagger \cdots d_{m_n}^\dagger |0\rangle$, carry quasi-angular momentum $m = (m_1 + \cdots + m_n) \bmod N$, where n is the number of particles. A discussion similar to the one given for bosons yields m as a function of rotation:

$$m = nj \bmod N; \quad j = 0, 1, 2, \dots; \quad n \text{ odd}, \quad (32)$$

$$m = n \left(j + \frac{1}{2} \right) \bmod N; \quad j = 0, 1, 2, \dots; \quad n \text{ even}. \quad (33)$$

As expected, the single-particle cases for both bosons and fermions are identical. It turns out that the cases of odd numbers of particles also coincide. However, there is an interesting distinction between the two cases when the number of particles in the system is even (compare equations 29 and 33). For instance, a system of two fermions in a four-site lattice cycles between quasi-angular momenta 1 and 3 whereas a system of two bosons cycles between values 2 and 4. This is one way in which non-interacting fermions and strongly-interacting bosons in one dimension differ despite the Jordan-Wigner transformation that maps between the two cases.

3.3. Non-interacting fermions in a two-dimensional square lattice

Differences between fermions and bosons remain when considering two-dimensional systems. Here we describe non-interacting fermions in a two-dimensional 4×4 square lattice.

The Hamiltonian can be written as the sum of three terms, $H = H_{12} + H_4 + V$, where H_{12} is the Hamiltonian of the outer twelve-site ring, H_4 is the Hamiltonian of the inner four-site ring, and V is the hopping between the rings,

$$V = - \sum_{\langle i, j \rangle} \left(t + \frac{M\Omega^2}{2} A_1 \right) a_i^{(12)\dagger} a_j^{(4)} e^{-i\phi_{ij}} + h.c., \quad (34)$$

where the superscripts 4 and 12 indicate whether site j is on the outer 12-site or inner 4-site ring. The Hamiltonians H_4 and H_{12} can be separately diagonalized (apart from the term in H_{12} involving r_i^2) via the transformations,

$$d_m^{(N)} = \frac{1}{\sqrt{N}} \sum_{j=1}^N e^{-i2\pi m j/N} a_j^{(N)}. \quad (35)$$

In figure 8(a) is plotted the single-particle energy spectrum for the Hamiltonian in the absence of hopping between the rings ($V = 0$). When the hopping is “turned on” (figure 8(b)), level crossings become avoided crossing due to the mixing of states with the same four-fold quasi-angular momentum. In figure 8(c), the case for zero hopping between rings is plotted for $\Omega = 0.05 E_R/\hbar$, whereas in figure 8(d), the hopping has turned on, and the avoided crossing behavior is observed.

In figure 9 are plotted the quasi-angular momenta of the ground state as a function of rotation speed for 1, 2, 3, 4, and 5 non-interacting fermions in a sixteen-site lattice. Similar to the ring lattice case, the results for odd numbers of particles are identical to those for hard-core bosons, but differ for even numbers of particles. However, there is an extra distinction that does not occur in the ring lattice. The pattern of m values taken on for five particles (see figure 9(e)) differs markedly from that of one particle (see figure 9(a)), whereas for bosons these patterns are essentially identical [30].

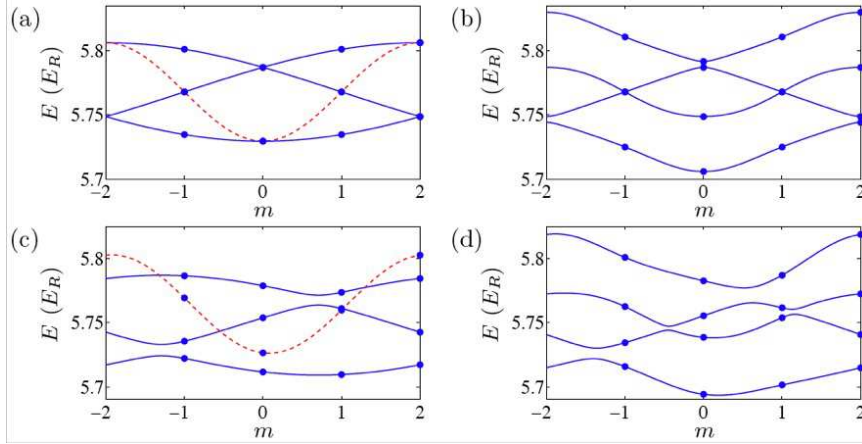


Figure 8. (Color online.) Single-particle energy spectrum in a 4×4 square lattice for (a) zero rotation and zero hopping between inner and outer rings, (b) zero rotation and non-zero hopping, (c) $\Omega = 0.05 E_R/\hbar$ and zero hopping, and (d) $\Omega = 0.05 E_R/\hbar$ and non-zero hopping between inner and outer rings. The dashed and solid line are aids to the eye that indicate the band. In (a) and (c), the red dashed line is the spectrum for the inner 4-site lattice.

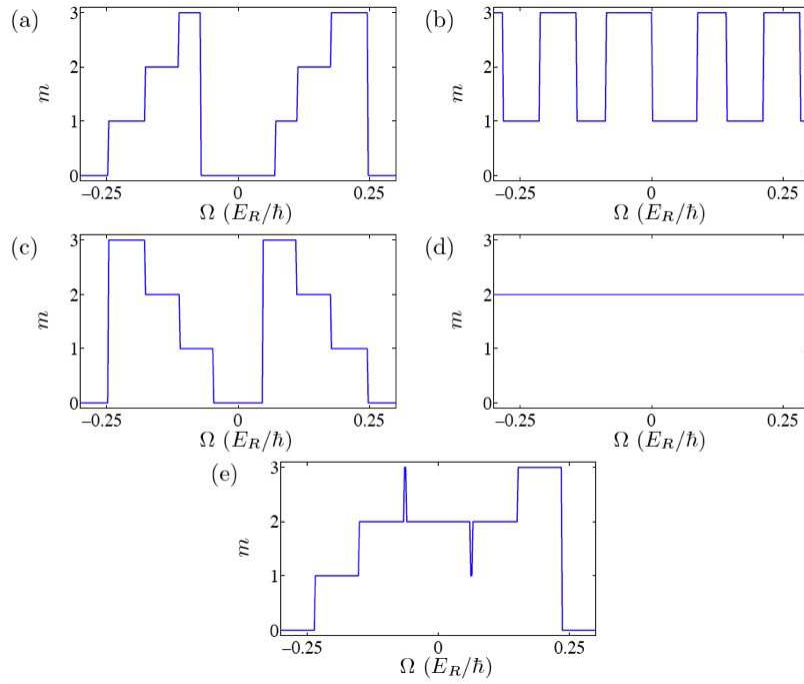


Figure 9. (Color online.) Quasi-angular momentum as a function of rotation for (a) 1, (b) 2, (c) 3, (d) 4, and (e) 5 non-interacting fermions in a sixteen site square lattice. These patterns repeat for larger rotation rates.

4. Signatures of quasi-angular momentum in the momentum distribution

While the quasi-angular momentum m is a good quantum number and a useful tool in investigating the symmetry properties of the ground state, it is not a quantity that can be directly measured in experiments. Instead, experiments are routinely performed in which time-of-flight, far-field, density images of the gas contain directly information about the momentum distribution before expansion. As a first step towards detecting quasi-angular momentum states, we look for a signature of quasi-angular momentum in the momentum distribution of a state.

The momentum distribution of the many-body state, $|\psi\rangle$, is given by

$$n(\mathbf{k}) = \langle \psi | \hat{\Psi}^\dagger(\mathbf{k}) \hat{\Psi}(\mathbf{k}) | \psi \rangle, \quad (36)$$

where $\hat{\Psi}(\mathbf{k})$ is the Fourier transform of the field operator $\hat{\Psi}(\mathbf{x})$. Recalling that we expand the field operators as

$$\hat{\Psi}(\mathbf{x}) = \sum_j a_j W_j(\mathbf{x}) = \sum_j a_j e^{-i\phi_{ij}} w(\mathbf{x} - \mathbf{x}_j), \quad (37)$$

it can be shown that the momentum distribution takes the form

$$n(\mathbf{k}) = \sum_{ll'} w^*(\mathbf{k}_l) w(\mathbf{k}_{l'}) e^{i\mathbf{k} \cdot (\mathbf{x}_l - \mathbf{x}_{l'})} \langle \psi | a_l^\dagger a_{l'} | \psi \rangle, \quad (38)$$

where

$$\mathbf{k}_l = \mathbf{k} + \Omega \frac{M}{\hbar} \mathbf{x}_l \times \hat{\mathbf{z}}. \quad (39)$$

This distribution is written in the momentum coordinates, \mathbf{k} , corresponding to the rotating frame coordinates, \mathbf{x} . Since the number density rotates in the lab frame coordinates, \mathbf{x}_L , the momentum distribution also rotates in the lab frame momentum coordinates, \mathbf{k}_L . However, far-field pictures of the gas will be snapshots of the momentum distribution at the moment the trap and lattice are turned off, provided the switch-off time is fast enough. Thus, the momentum distributions presented here are accurate representations of what will be measured in time-of-flight measurements, although they may be rotated relative to each other.

Since quasi-angular momentum is a reflection of the symmetry of the system, considering single-particle states should be sufficient to capture the basics of how this quantum number affects the momentum distribution. We therefore concentrate on single-particle states only. In this case, $n(\mathbf{k})$ is merely the square of the Fourier transform of the wavefunction.

In order to build up an understanding of the momentum distribution, first drop the Wannier functions. In this case, $n(\mathbf{k})$ is the Fourier transform of a sum of weighted delta functions. On a four site-lattice, the wavefunction is of the form

$$\psi(\mathbf{x}) = \sum_{j=1}^4 e^{i2\pi m j/4} \delta(\mathbf{x} - \mathbf{x}_j), \quad (40)$$

where \mathbf{x}_j are the four corners of a square centered at $\mathbf{x} = 0$. In figure 10 are plotted the momentum distributions for $m = 0, 1$, and 2 . The $m = 0$ is peaked at $\mathbf{k} = 2\pi n/d$, with n an integer and d the lattice spacing, whereas the other states vanish at these points. The spacing between peaks for both $m = 0$ and $m = 2$ is $\Delta k = 2\pi/d$, whereas for $m = 1, 3$ this spacing is $\Delta k = 2\pi/\sqrt{2}d$; these can be calculated analytically. Thus, since the lattice spacing is known, there are clear measurable distinctions between

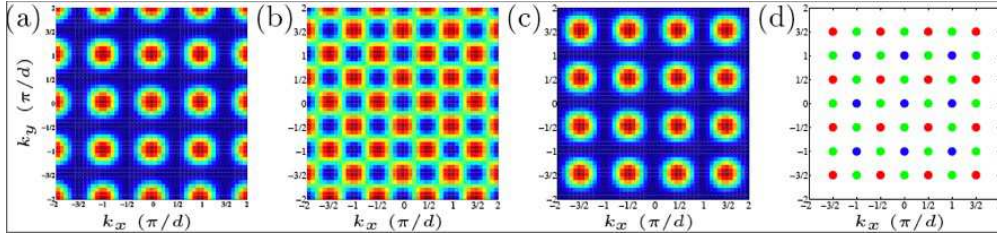


Figure 10. (Color online.) Fourier transform of generic (a) $m = 0$, (b) $m = 1, 3$, and (c) $m = 2$ quasi-angular momentum states on four sites. These momentum distributions are plotted over a range $4\pi/d \leq k_x, k_y \leq 4\pi/d$; the first Brillouin zone is given by $\pi/d \leq k_x, k_y \leq \pi/d$. (d) A schematic of the peak structure of four delta functions of the $m = 0$ (blue), $m = 1, 3$ (green), and $m = 2$ (red) quasi-angular momentum states. The peak spacings for the $m = 0$ and $m = 2$ states are both $2\pi/d$, where d is the spacing between the delta functions, whereas the peak spacing for $m = 1, 3$ is $2\pi/\sqrt{2}d$.

different generic quasi-angular momentum states. Note that $m = 1$ and $m = 3$ are identical as they represent similar states with counter-propagating current patterns.

Re-including the Wannier functions contributes to the momentum distribution an overall envelope of approximate width $\sqrt{V/E_R}/4$, where V is the depth of the lattice. The modification $\mathbf{k} \rightarrow \mathbf{k}_l$, equation 39, moves the peak of this envelope away from $\mathbf{k} = 0$ as rotation is increased, though the center of the envelope is always located at $\mathbf{k} = 0$. This is consistent with higher momenta being accessed for higher rotation rates.

At this point, it is important to note that locating $\mathbf{k} = 0$ in the distribution is necessary for distinguishing the $m = 0$ and $m = 2$ states. This can be done easily due to the overall envelope in momentum space that is centered at $\mathbf{k} = 0$.

There are two additional considerations that come into play for larger lattices, both system-size effects. An overall envelope in position space determines the width of the peaks in momentum space. This envelope determines the size of the system, and if the width is roughly L , then the width of the peaks in momentum space scales as $1/L$. If the lattice spacing is increased by a factor of n , then the peak-spacing in momentum space is decreased by a factor of $1/n$. The general peak structure is not modified by these considerations.

Since the peak structure is not modified by lattice-size effects, we can conclude that the distinctions between quasi-angular momentum states are sustained for more physical systems, which we turn to next. The ground state momentum distribution for a one-hundred-site lattice in the presence of a harmonic trap of frequency $\Omega_T = 0.15E_R/\hbar$ is computed via imaginary time propagation. The trap ensures that the majority of the number density resides on the inner 36 sites.

The results are summarized in figure 11, in which are plotted the momentum distributions for $m = 0, 1$, and, 2 states at rotation speeds of $0, 0.1E_R/\hbar$, and $0.145E_R/\hbar$, increasing to the right. We can again make the observation that the $m = 0$ state is the only one that is non-zero at exactly the reciprocal lattice vectors, i.e. $\mathbf{k} = \frac{2\pi n}{d}\hat{\mathbf{k}}_x + \frac{2\pi m}{d}\hat{\mathbf{k}}_y$. The peak-spacing is smaller for the $m = 1$ state than for the $m = 2$ state, distinguishing them from each other. However, the exact peak-spacing is unclear due to complex interference effects between sites at different radii.

These differences are washed out at higher rotation speeds. The $m = 1$,

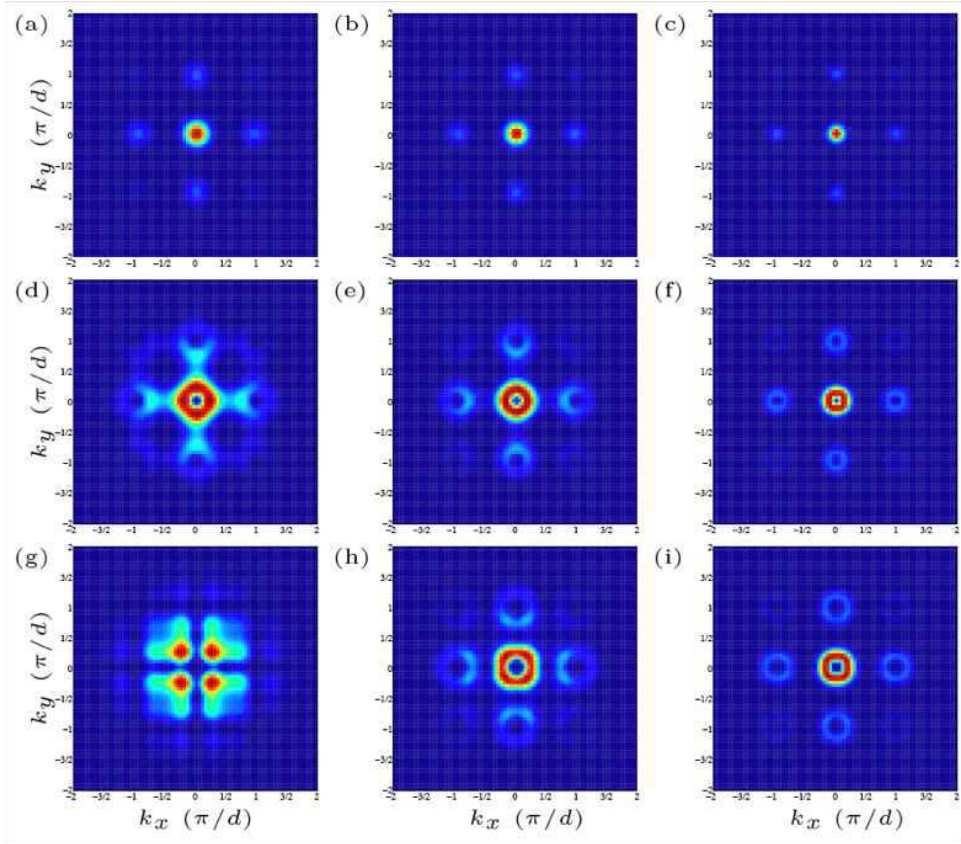


Figure 11. (Color online.) Momentum distributions computed via imaginary time propagation for one particle in a 100-site lattice in the presence of a trap of frequency $\Omega_T = 0.15E_R/\hbar$. Plotted are $m = 0$ ((a), (b), and (c)), $m = 1$ ((d), (e), and (f)), and $m = 2$ ((g), (h), and (i)) states for rotation speeds of $\Omega = 0$ ((a), (d), and (g)), $\Omega = 0.1E_R/\hbar$ ((b), (e), and (h)), and $\Omega = 0.145E_R/\hbar$ ((c), (f), and (i)). At zero rotation, the distinctions between different quasi-angular momenta are sustained. As rotation is increased, it becomes harder to distinguish $m = 1$ and $m = 2$ states. Due to the centrifugal term, higher rotation increases the width of the envelope of the number density, decreasing the width of the peaks in momentum space. Not shown is $m = 3$ which has a structure similar to both $m = 1$ and $m = 2$ for large rotation but has a ring-radius larger than both of them.

$m = 2$, and $m = 3$ (not pictured) states have very similar structures for large rotation. The peaks overlap so that it is very difficult to resolve them; the momentum distributions then all appear to be rings centered at reciprocal lattice vectors. They are distinguishable via the radius of the ring, as the radius is smallest for $m = 1$ and largest for $m = 3$, but as this is in order of increasing energy, the larger radius may just be an artifact of the larger width in the number density envelope at higher energies. Indeed, figures 11a, 11b, and 11c are consistent with this conclusion, as the momentum peaks are narrowing due to the number density spreading out in real space. These results are consistent with those calculated via direct diagonalization of the Hubbard models previously discussed.

5. Conclusion

By analogy with quasi-momentum in translationally invariant periodic systems, the notion of quasi-angular momentum was introduced to label the eigenstates of a Hamiltonian that has a discrete rotational symmetry. It was shown that quasi-angular momentum is useful in analyzing the ground-state properties of quantum gases of bosons or fermions in rotating optical lattices. In particular, monitoring the quasi-angular momentum of the ground state as a function of rotation allowed us to identify transitions between different circulation values.

We also presented a possible avenue by which the quasi-angular momentum of a state can be experimentally determined. We identified characteristics in the momentum distribution distinguishing between different quasi-angular momentum states at low rotation speeds, such as the existence of a peak at reciprocal lattice vectors for an $m = 0$ state only, the peak-spacing, and the overall structure of the momentum distribution.

There are still open questions as to how the momentum distributions will change when the lattice size or number of particles is increased. The effects of statistics will be of fundamental importance for many-particle systems; there is a question of how well the peaks can be resolved for larger lattices, since peak-spacing decreases with increasing lattice size; and interference effects between adjacent sites and between rings is not rigorously treatable. However, there will always be signatures of the quasi-angular momentum in the momentum distribution, as it is connected with the phase information of the ground state, which in turn influences the momenta of the system. In addition, a zero quasi-angular momentum state can be distinguished from a non-zero one, which allows the experimenter to verify that vorticity has entered the system.

Acknowledgements

We acknowledge extremely useful discussions with both Brian Seaman and John Cooper. The authors would also like to acknowledge funding support from the Department of Energy, Office of Basic Energy Sciences via the Chemical Sciences, Geosciences, and Biosciences Division, NASA, and Deutsche Forschungsgemeinschaft (MK).

Appendix

The case of fillings between l and $l + 1$ can be encoded in the Hamiltonian by formally changing the properties of the creation and annihilation operators. As mentioned in the body of the paper, for fillings less than one, the creation and annihilation operators satisfy the following relations:

$$\{a_i, a_i^\dagger\} = 1, \quad [a_i, a_j] = [a_i, a_j^\dagger] = 0. \quad (\text{A.1})$$

If the filling fraction is between l and $l + 1$, the following changes are made. First, the site number operator $a_j^\dagger a_j$ is replaced by $a_j^\dagger a_j + l$, reflecting the fact that each site is filled with between l and $l + 1$ particles. Secondly, recalling that the operators were originally bosonic, $a_j^\dagger |l\rangle = \sqrt{l+1} |l+1\rangle$ and $a_j |l+1\rangle = \sqrt{l+1} |l\rangle$, one can see that

the hopping parameter t is scaled by a factor of $l + 1$. Finally, the interaction term gets modified according to the replacement $a_j^\dagger a_j \rightarrow a_j^\dagger a_j + l$:

$$\sum_{j=1}^N a_j^\dagger a_j (a_j^\dagger a_j - 1) \rightarrow 2l \sum_{j=1}^N a_j^\dagger a_j + Nl(l-1) \quad (\text{A.2})$$

The Hamiltonian in two-state approximation is then given by

$$H = (Ul - \mu) \sum_{j=1}^N a_j^\dagger a_j - \mu Nl + UN \frac{l(l-1)}{2} - (l+1) \sum_{j=1}^N t e^{i\phi} a_{j+1}^\dagger a_j + h.c. \quad (\text{A.3})$$

where the chemical potential μ has been introduced so that we can work in the grand-canonical ensemble.

Upon applying the Jordan-Wigner transformation,

$$b_j = a_j e^{i\pi \sum_{k=1}^{j-1} a_k^\dagger a_k}, \quad (\text{A.4})$$

the Hamiltonian becomes

$$H = (Ul - \mu) \sum_{j=1}^N b_j^\dagger b_j - \mu Nl + UN \frac{l(l-1)}{2} - (l+1) \sum_{j=1}^{N-1} t e^{i\phi} b_{j+1}^\dagger b_j + h.c. \\ - (-1)^{n+1} (l+1) t e^{i\phi} b_1^\dagger b_N + h.c. \quad (\text{A.5})$$

where n is the number of particles. Now that the Hamiltonian is fully fermionic, we can perform a canonical transformation to diagonalize it,

$$d_m = \frac{1}{\sqrt{N}} \sum_{k=1}^N e^{i\pi f_m k/N} b_k, \quad (\text{A.6})$$

where $f_m = 2m$ for n odd and $f_m = 2m - 1$ for n even. The resulting Hamiltonian is

$$H = -\mu Nl + \frac{U}{2} Nl(l-1) + \sum_{m=1}^N E_m d_m^\dagger d_m, \\ E_m = -\mu - 2(l+1)t \cos\left(\frac{\pi f_m}{N} - \phi\right) + Ul. \quad (\text{A.7})$$

Setting l and μ to zero, we realize the Hamiltonian derived in Sec. 3.

As an aside, this calculation actually yields more than just the description of the quasi-angular momentum of a rotating ring lattice. In the limit of large N , this system is indistinguishable from a linear lattice. Taking t real, the Mott-insulator/superfluid phase diagram in two-state approximation can be derived. Allowing the number of particles to vary, it is apparent that the number of particles is determined by the number of m 's for which $E_m < 0$. Varying the chemical potential μ , every time there exists an m such that $E_m = 0$, there is a phase boundary between ground states of different numbers of particles. Thus, the phase boundaries are given by the expression,

$$\frac{\mu}{U} = -2(l+1) \frac{t}{U} \cos\left(\frac{\pi f_m}{N}\right) + l. \quad (\text{A.8})$$

In particular, it is possible to identify regions of integer filling and non-integer filling, the boundaries between which are given by

$$\frac{\mu}{U} = \pm 2(l+1) \frac{t}{U} + l \quad (\text{A.9})$$

for a large number of sites. These boundaries yield an approximation to the Mott-insulator superfluid phase diagram (figure A1). We note that this method can be easily extended to the case of superlattices, generating for instance Mott phases of half-filling in the phase diagram.

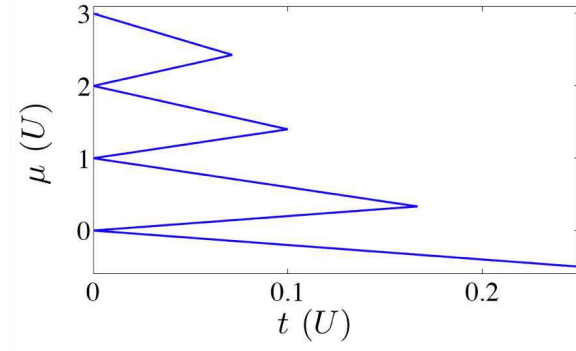


Figure A1. (Color online.) Bose-Hubbard phase diagram for an infinite one-dimensional lattice in two-state approximation.

References

- [1] MH Anderson, JR Ensher, MR Matthews, CE Wieman, and EA Cornell. Observation of Bose-Einstein Condensation in a Dilute Atomic Vapor. *Science*, 269(5221):198, 1995.
- [2] KB Davis, MO Mewes, MR Andrews, NJ van Druten, DS Durfee, DM Kurn, and W Ketterle. Bose-Einstein Condensation in a Gas of Sodium Atoms. *Physical Review Letters*, 75(22):3969–3973, 1995.
- [3] CC Bradley, CA Sackett, JJ Tollett, and RG Hulet. Evidence of Bose-Einstein Condensation in an Atomic Gas with Attractive Interactions. *Physical Review Letters*, 75(9):1687–1690, 1995.
- [4] B DeMarco and DS Jin. Onset of Fermi Degeneracy in a Trapped Atomic Gas. *Science*, 285(5434):1703–1706, 1999.
- [5] MW Zwierlein, JR Abo-Shaer, A Schirotzek, CH Schunck, and W Ketterle. Vortices and superfluidity in a strongly interacting Fermi gas. *Nature*, 435:1047–1051, 2005.
- [6] M Greiner, CA Regal, and DS Jin. Emergence of a molecular Bose-Einstein condensate from a Fermi gas. *Nature*, 426(6966):537–540, 2003.
- [7] JN Milstein, S Kokkelmans, and MJ Holland. Resonance theory of the crossover from Bardeen-Cooper-Schrieffer superfluidity to Bose-Einstein condensation in a dilute Fermi gas. *Physical Review A*, 66(4):43604, 2002.
- [8] MPA Fisher, PB Weichman, G Grinstein, and DS Fisher. Boson localization and the superfluid-insulator transition. *Phys. Rev. B*, 40(1):546–570, Jul 1989.
- [9] M Greiner, O Mandel, T Esslinger, TW Hänsch, and I Bloch. Quantum phase transition from a superfluid to a Mott insulator in a gas of ultracold atoms. *Nature*, 415:39–44, 2002.
- [10] NK Wilkin and JMF Gunn. Condensation of “composite bosons” in a rotating bec. *Phys. Rev. Lett.*, 84(1):6–9, Jan 2000.
- [11] B Paredes, P Fedichev, JI Cirac, and P Zoller. $\frac{1}{2}$ -anyons in small atomic bose-einstein condensates. *Phys. Rev. Lett.*, 87(1):010402, Jun 2001.
- [12] UR Fischer, PO Fedichev, and A Recati. Vortex liquids and vortex quantum Hall states in trapped rotating Bose gases. *J. Phys. B.*, 37:S301, 2004.
- [13] MA Baranov, K Osterloh, and M Lewenstein. Fractional quantum hall states in ultracold rapidly rotating dipolar fermi gases. *Phys. Rev. Lett.*, 94(7):070404, 2005.
- [14] V Schweikhard, I Coddington, P Engels, VP Mogendorff, and EA Cornell. Rapidly rotating bose-einstein condensates in and near the lowest landau level. *Phys. Rev. Lett.*, 92(4):040404, 2004.
- [15] D Jaksch and P Zoller. Creation of effective magnetic fields in optical lattices: the Hofstadter butterfly for cold neutral atoms. *New J. Phys.*, 5(1):56, 2003.
- [16] RN Palmer and D Jaksch. High-Field Fractional Quantum Hall Effect in Optical Lattices. *Phys. Rev. Lett.*, 96(18):180407, 2006.
- [17] AS Sørensen, E Demler, and MD Lukin. Fractional Quantum Hall States of Atoms in Optical Lattices. *Phys. Rev. Lett.*, 94(8):86803, 2005.
- [18] R Bhat, M Krämer, J Cooper, and MJ Holland. Hall effects in Bose-Einstein condensates in a rotating optical lattice. *Arxiv preprint arXiv:0705.3341v1*, 2007.

- [19] M Hafezi, AS Sorensen, E Demler, and MD Lukin. Fractional Quantum Hall Effect in Optical Lattices. *Arxiv preprint arXiv:0706.0757v1*, 2007.
- [20] AM Rey, K Burnett, II Satija, and CW Clark. Lifshitz-like transition and enhancement of correlations in a rotating bosonic ring lattice. *Arxiv preprint cond-mat/0611332*, 2006.
- [21] P Vignolo, R Fazio, and MP Tosi. Quantum vortices in optical lattices. *Arxiv preprint arXiv:cond-mat/0701439v1*, 2007.
- [22] R Bhat, MJ Holland, and LD Carr. Bose-Einstein Condensates in Rotating Lattices. *Phys. Rev. Lett.*, 96(6):60405, 2006.
- [23] S Reich, C Thomsen, J Maultzsch, and M Janina. *Carbon Nanotubes: Basic Concepts and Physical Properties*. Wiley-VCH, 2004.
- [24] MP Marder. *Condensed Matter Physics*. Wiley, New York, 2000.
- [25] C Kittel. *Introduction to Solid State Physics*. Wiley, New York, 1996.
- [26] LD Landau and EM Lifshitz. *Mechanics*. Butterworth-Heinemann, Ltd, Oxford, 1976.
- [27] M. Girardeau. Relationship between Systems of Impenetrable Bosons and Fermions in One Dimension. *Journal of Mathematical Physics*, 1:516, 2004.
- [28] E.H. Lieb and W. Liniger. Exact Analysis of an Interacting Bose Gas. I. The General Solution and the Ground State. *Physical Review*, 130(4):1605–1616, 1963.
- [29] D Jaksch, C Bruder, JI Cirac, CW Gardiner, and P Zoller. Cold Bosonic Atoms in Optical Lattices. *Phys. Rev. Lett.*, 81(15):3108–3111, 1998.
- [30] R Bhat, BM Peden, BT Seaman, M Krämer, LD Carr, and MJ Holland. Quantized Vortex States of Strongly Interacting Bosons in a Rotating Optical Lattice. *Phys. Rev. A*, 74:063606, 2006.
- [31] P Jordan and E Wigner. Über das Paulische Äquivalenzverbot. *Z. Phys.*, 47:631, 1928.
- [32] TD Schultz. Note on the One-Dimensional Gas of Impenetrable Point-Particle Bosons. *J. Math. Phys.*, 4:666, 1966.